Journal of Materials Science: Materials in Electronics

PLZT Film Capacitors for Power Electronics and Energy Storage Applications

--Manuscript Draft--

Manuscript Number:	JMSE-D-14-01590R2
Full Title:	PLZT Film Capacitors for Power Electronics and Energy Storage Applications
Article Type:	S.I. : Electronic Materials for Harsh Environments
Keywords:	Ferroelectricity; PLZT; ceramic film capacitor; energy storage; residual stress
Corresponding Author:	Beihai Ma, PhD Argonne National Laboratory Lemont, IL UNITED STATES
Corresponding Author Secondary Information:	
Corresponding Author's Institution:	Argonne National Laboratory
Corresponding Author's Secondary Institution:	
First Author:	Beihai Ma, PhD
First Author Secondary Information:	
Order of Authors:	Beihai Ma, PhD
	Zhongqiang Hu, PhD
	Rachel E. Koritala, PhD
	Tae H. Lee, PhD
	Stephen E. Dorris, PhD
	Uthamalingam Balachandran, PhD
Order of Authors Secondary Information:	
Abstract:	Ceramic film capacitors with high dielectric constant and high breakdown strength hold special promise for applications demanding high power density. By means of chemical solution deposition, we deposited ≈2-μm-thick films of lanthanum-doped lead zirconate titanate (PLZT) on $LaNiO_3$-buffered Ni (LNO/Ni) foils and platinized silicon (PtSi) substrates. The dielectric properties and energy storage performance of the resulting samples were determined under a high level of applied electric field. X-ray diffraction stress analysis revealed that PLZT on LNO/Ni bears a compressive stress of ≈370 MPa while PLZT on PtSi endures a tensile stress of ≈250 MPa. Compressive stress was found to lead to heightened polarization, improved tunability, increased irreversible domain wall motion, and enhanced breakdown strength for PLZT deposited on the LNO/Ni as compared with the PtSi substrate. We observed a tunability of ≈55% and ≈40% at room temperature under 100 kV/cm applied field, remanent polarization of ≈23.5 μC/cm² and ≈7.4 μC/cm², coercive electric field of ≈25.6 kV/cm and ≈21.1 kV/cm, and dielectric breakdown strength of ≈2.6 MV/cm and ≈1.5 MV/cm for PLZT deposited on LNO/Ni foils and PtSi substrates, respectively. A high recoverable energy density of ≈85 J/cm³ and energy conversion efficiency of ≈65% were measured on the PLZT film grown on LNO/Ni.

PLZT Film Capacitors for Power Electronics and Energy Storage Applications*

Beihai Ma[1], Zhongqiang Hu[1,2], Rachel E. Koritala[3], Tae H. Lee[1], Stephen E. Dorris[1], and Uthamalingam (Balu) Balachandran[1]

[1]Energy Systems Division, Argonne National Laboratory, Argonne, IL 60439

[2]Current Address: Electrical and Computer Engineering Department, Northeastern University, Boston, MA 02115

[3]Nanoscience and Technology Division, Argonne National Laboratory, Argonne, IL 60439

November 2014

(Revised March 2015)

For submittal to the Journal of Materials Science - Materials in Electronics.

* This work was supported by the U.S. Department of Energy, Vehicle Technologies Program, under Contract DE-AC02-06CH11357.

PLZT Film Capacitors for Power Electronics and Energy Storage Applications

Beihai Ma[1], Zhongqiang Hu[1,2], Rachel E. Koritala[3], Tae H. Lee[1], Stephen E. Dorris[1], and Uthamalingam (Balu) Balachandran[1]

[1]Energy Systems Division, Argonne National Laboratory, Argonne, IL 60439

[2]Current Address: Electrical and Computer Engineering Department, Northeastern University, Boston, MA 02115

[3]Nanoscience and Technology Division, Argonne National Laboratory, Argonne, IL 60439

Abstract

Ceramic film capacitors with high dielectric constant and high breakdown strength hold special promise for applications demanding high power density. By means of chemical solution deposition, we deposited ≈2-μm-thick films of lanthanum-doped lead zirconate titanate (PLZT) on $LaNiO_3$-buffered Ni (LNO/Ni) foils and platinized silicon (PtSi) substrates. The dielectric properties and energy storage performance of the resulting samples were determined under a high level of applied electric field. X-ray diffraction stress analysis revealed that PLZT on LNO/Ni bears a compressive stress of ≈370 MPa while PLZT on PtSi endures a tensile stress of ≈250 MPa. Compressive stress was found to lead to heightened polarization, improved tunability, increased irreversible domain wall motion, and enhanced breakdown strength for PLZT deposited on the LNO/Ni as compared with the PtSi substrate. We observed a tunability of ≈55% and ≈40% at room temperature under 100 kV/cm applied field, remanent polarization of ≈23.5 μC/cm^2 and ≈7.4 μC/cm^2, coercive electric field of ≈25.6 kV/cm and ≈21.1 kV/cm, and dielectric breakdown strength of ≈2.6 MV/cm and ≈1.5 MV/cm for PLZT deposited on LNO/Ni foils and PtSi substrates, respectively. A high recoverable energy density of ≈85 J/cm^3 and energy conversion efficiency of ≈65% were measured on the PLZT film grown on LNO/Ni.

Keywords: Ferroelectricity, PLZT, ceramic film capacitor, energy storage, residual stress

PACS code: 77.22.Jp, 77.55.-g, 77.55.fg, 77.80.bn, 77.80.Jk

Introduction

In recent years, the advancement in ceramic film capacitor technology has attracted significant research interest in developing electronic materials for applications at elevated temperatures to realize the benefit of better operational efficiencies [1-4]. Capacitors are essential for carrying out a host of functions in pulse power and power electronics applications such as pulse discharge, filtering, voltage smoothing, coupling, de-coupling, DC blocking, power conditioning, snubbing, electromagnetic interference suppression, and commutation in power electronics. Specific requirements need to be satisfied according to their intended applications. For example, snubber capacitors are used for minimizing power dissipation in silicon and silicon carbide based switching devices and for power smoothing in switch-mode power supplies. They typically possess small capacitance (10 nF to 1 μF), operate at high frequency (10 kHz to 1 MHz), and are placed close to the switch, which they protect. The snubber capacitor experiences full voltage transients, from 0 V to the bus voltage. Therefore, dielectric materials with low hysteresis losses are essential. Snubber capacitors are designed for low self-inductance and high ripple current handling. On the other hand, bus capacitors act as an energy source to stabilize the DC bus voltage in power electronic circuits such as DC/AC inverters of hybrid electric systems. Bus capacitors possess large capacitance (100 - 2000 μF) and operate under a stable DC bias with a superimposed AC transient voltage. Bus capacitors are generally the largest capacitors in the power electronic circuit, and high-energy density is very important. Filter capacitors are used to remove the spurious signals from the fundamental output frequency and are placed at the inverter output. Dielectrics for filter capacitors must also be linear with low hysteresis loss. The energy storage capacity of a capacitor is proportional to the production of the applied electric field and the resulting dielectric polarization [5,6]. Ideally, for power electronic applications, capacitor materials would have high breakdown strength, high permittivity, low dielectric losses, low electronic and ionic conductivities, and minimal thermal runaway.

Ceramic capacitors are promising for high temperature applications that require swift delivery of large amounts of electric energy. Capacitors in DC/AC inverters of hybrid electric systems are required to have not only high energy storage density, but also high-power electric output and high temperature operation [7,8]. Currently available commercial DC bus capacitors, made from polypropylene, do not possess the high temperature performance required for use in

future electric-drive vehicle systems. Their performance deteriorates rapidly at temperatures above 85°C. Therefore, they require a separate secondary cooling system that operates at lower temperature to ensure appropriate ripple current handling. This secondary cooling system leads to added payload and increased cost of operation. Utilizing the primary engine cooling system for operation at higher temperature (≈140°C) is highly desirable for the next generation invertor for use on electric-drive vehicles. Elimination of the secondary cooling system dedicated for the inverter can substantially reduce the cost and overall weight. To achieve this objective, capacitors that are capable of operating at high temperature (>140°C) are in demand.

Recently, high-temperature polymer ferroelectrics, ceramic ferroelectrics, antiferroelectrics, and relaxor ferroelectrics have shown better potential and higher energy density than those of linear dielectrics [5,6,9-12]. Chu et al. reported high dielectric breakdown strength and high energy density of ≈17 J/cm^3 in the poly[(vinylidenefluoride-co-trifluoroethylene] [P(VDF-TrFE)] copolymer, where the introduction of defects converts this material to a relaxor ferroelectric with almost negligible remanent polarization [5]. Yao et al. reported a series of relaxor-antiferroelectric thin films, relaxor-ferroelectric thin films, and PVDF-based polymer blend thin films that show high energy density (10 to 25 J/cm^3) [9]. Ma et al. reported an energy density of ≈53 J/cm^3 in PLZT films grown on metal foils [10,12]. Hao et al. reported an energy density of ≈30 J/cm^3 in relaxor ferroelectric PLZT films grown on platinized silicon substrates [11]. Hu et al. reported recoverable energy density of ≈60 J/cm^3 in antiferroelectric PLZT film capacitors [6]. These advanced capacitor materials signify the potential for energy storage and conversion applications. In this paper, we report our recent development of PLZT film capacitors for power electronics and high-field energy storage.

Experiment

Platinized silicon (PtSi) substrates were cut from premium-grade <100> oriented silicon wafers of ≈375-μm-thick silicon with 500-nm-thick thermally oxidized silicon dioxide coated with 20-nm-thick titanium and 200-nm-thick platinum. The wafers were acquired from Nova Electronic Materials (Flower Mound, TX). High purity (99.98% pure) nickel substrates, 25-mm square and 0.4-mm thick (obtained from MTI Corp., Richmond, CA), were polished by

chemical-mechanical planarization (CMP). Prior to coating, the substrates were cleaned in acetone and methanol in sequence and blow dried with nitrogen.

Lanthanum-doped lead zirconate titanate (PLZT) precursor solutions of 0.5 M concentration and lanthanum nickel oxide (LNO) precursor solutions of 0.2 M concentration were prepared by a modified 2-methoxyethanol synthesis route [13,14] using an appropriate amount of titanium isopropoxide, zirconium n-propoxide, lead acetate trihydrate, lanthanum nitrate hexahydrate, and nickel acetate tetrahydrate (all from Sigma-Aldrich, St. Louis, MO). The PLZT solutions contained 20 mol.% excess lead to compensate for lead loss during the heat treatment process described below. All solutions were refluxed for at least 2 hours inside a nitrogen-filled glove box and then filtered through Restek polytetrafluoroethylene syringe filters (Restek Corp., Bellefonte, PA) with 0.22-μm open pore size before being used for coating.

Chemical-mechanical polished nickel was used as a substrate, which was coated with a LNO buffer film of ≈0.4 μm by chemical solution process prior to the deposition of PLZT. The filtered LNO precursor solution was spin coated with a Laurell WS400 spin processor (Laurell Technologies, North Wales, PA) at 3000 rpm for 30 s on Ni substrates, pyrolyzed at 450°C for 5 min, and annealed at 625°C for 2-5 min in air. This process was repeated three times to build the desired ≈0.4-μm-thick LNO buffer film.

Next, PLZT films were deposited on both PtSi or LNO-buffered nickel (LNO/Ni) substrates by the following process. Filtered PLZT precursor solution was spin coated on the LNO-buffered Ni substrates at 3000 rpm for 30 s, followed by pyrolysis at 450°C for 5 min and annealing at 650°C for 5-10 min for each coating. After every three layers of coating, additional annealing was performed at 650°C for 15 min. Solution coating and firing were repeated to produce films of desired thickness of ≈2 μm. All pyrolysis and annealing were performed in air in Lindburg tube furnaces. Each coating resulted in a PLZT film of ≈0.115-μm thickness after pyrolysis and crystallization.

The films were characterized by various analytical techniques. Film thickness was determined from cross-sectional images with scanning electron microscopy [14]. X-ray

diffraction (XRD) patterns were measured by a Bruker AXS D8 Discover with GADDS diffraction system. Platinum (Pt) top electrodes with thickness of 100 nm were deposited on the PLZT films by electron-beam evaporation through a shadow mask to define ≈250-μm-diameter capacitors. The samples with Pt top electrodes were annealed at 450°C in air for 2 min for electrode conditioning. A Signatone QuieTemp® probe system with heatable vacuum chuck (Lucas Signatone Corp., Gilroy, CA) was used for electrical characterization. For the electrical measurements, the Pt/PLZT/LNO/Ni heterostructure was contacted by a Pt top electrode pad with one probe and the substrate (bottom electrode) with the other. A positive applied voltage corresponds to a configuration where the top electrode is at a higher potential than the bottom electrode. An Agilent E4980A precision LCR meter was used to determine the capacitance and dissipation factor under an applied bias field. A Radiant Technologies Precision Premier II tester measured the hysteresis loops. The capacitor samples were immersed in Fluka silicone oil (Sigma-Aldrich) during measurements of high-field hysteresis loops and dielectric breakdown. A Keithley 237 high-voltage source meter was used to measure the current-voltage characteristics and the breakdown voltage was determined from 1 μV criterion [15].

Results and Discussion

Figure 1 shows the X-ray diffraction (XRD) patterns measured on the ≈2-μm-thick PLZT films deposited on LNO/Ni and PtSi substrates. The patterns indicate that both samples are well crystallized without preferred orientation. The diffraction peaks can be indexed according to a pseudo-cubic perovskite system (JCPDS 56-0900). The use of the LNO buffer layer effectively reduces the crystallization temperature and facilitates the formation of pyrochlore-free PLZT phase [16,17]. The LNO also compensates for the roughness of the Ni foil and provides a smooth interface for the PLZT film to grow on. Diffraction peaks from the nickel substrate and the LNO buffer film can be identified from the XRD pattern shown in Fig. 1a. The tiny peak at $2\theta \approx 36°$ on the XRD pattern for PLZT grown on PtSi (Fig. 1b) is from Cu-K_β diffraction of Pt (111). No crack or delamination was observed from microscopic analysis [14]. A close look at the two diffraction patterns in Fig. 1 reveals that the PLZT peaks in Fig. 1a shift to lower angle when compared to those peaks for the same index shown in Fig. 1b. With the regular θ-2θ scan configuration, diffraction patterns are measured on these crystallites with the diffraction planes

parallel to the substrate surface. According to Bragg's equation, a peak shift to lower 2θ angle indicates an expansion of d-spacing in the out-of-plane direction, which is a result of compressive strain in the in-plane directions that are parallel to the substrate surface. Residual stress analysis by XRD indicated compressive stress in the PLZT grown on the LNO-buffered nickel substrate and tensile strain in the PLZT grown on PtSi substrate, as a result of the difference in the coefficients of thermal expansion [18].

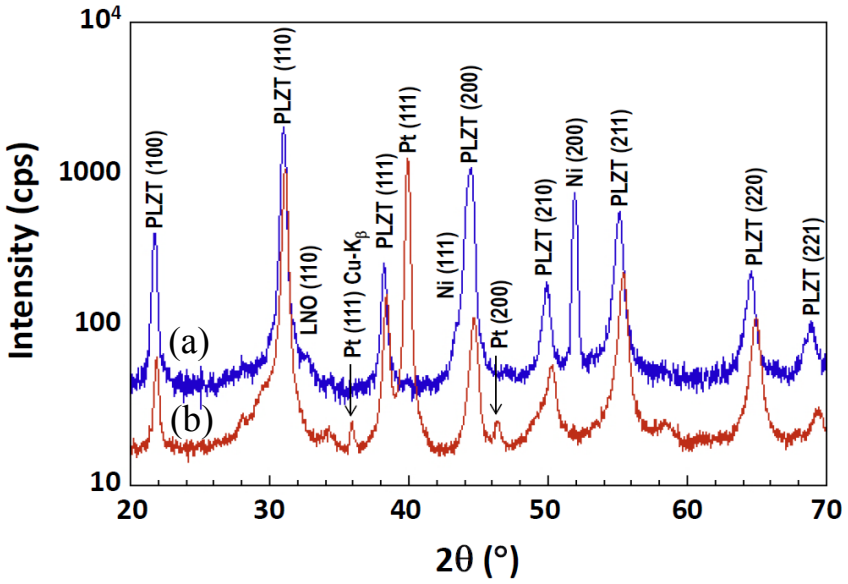

Figure 1. XRD patterns of PLZT grown on (a) LNO/Ni and (b) PtSi substrates.

To determine the residual stress in the PLZT films grown on LNO-buffered nickel and PtSi substrates, we obtained 2θ XRD patterns with various tilt angles ψ. Such residual stress in the PLZT films can be determined from XRD data measured under various tilt angles using the following equation [19],

$$\sigma_{\varphi} = \left(\frac{E}{1+\nu}\right)_{(hkl)} \cdot \frac{1}{d_{\varphi 0}} \cdot \frac{\partial d_{\varphi\psi}}{\partial \sin^2 \psi} \qquad (1)$$

where E and ν are Young's modulus and the Poisson ratio of the thin film, and $d_{\phi 0}$ and $d_{\phi\psi}$ are the lattice d-spacing in a stress-free and a stressed sample that was tilted at angle ψ, respectively. Young's modulus E = 72 GPa and Poisson ratio ν = 0.30 [20,21] were used in our calculation of the residual stress in the PLZT films. We measured XRD patterns at various rotation angles (ϕ = 0°, 45°, and 90°) and observed no measurable difference. This finding

indicates that crystallites in the polycrystalline films are homogeneous and randomly oriented without preferred orientation with respect to in-plane direction. Figure 2 shows lattice d-spacing as a function of $\sin^2\psi$ measured by XRD on PLZT films grown on the LNO/Ni and PtSi substrates. Data measured from the PLZT (211) and (220) diffraction peaks are plotted in Figs. 2a and 2b, respectively. Slopes determined from linear fitting to the data were plugged into Eq. 1 to determine the residual stresses in the PLZT films. We measured compressive stress of ≈370 MPa and tensile stress of ≈250 MPa, respectively, for the ≈2-μm-thick PLZT films grown on LNO buffered Ni and PtSi substrates. Our measurements of residual stresses are in good agreement with those reported for PZT films [20].

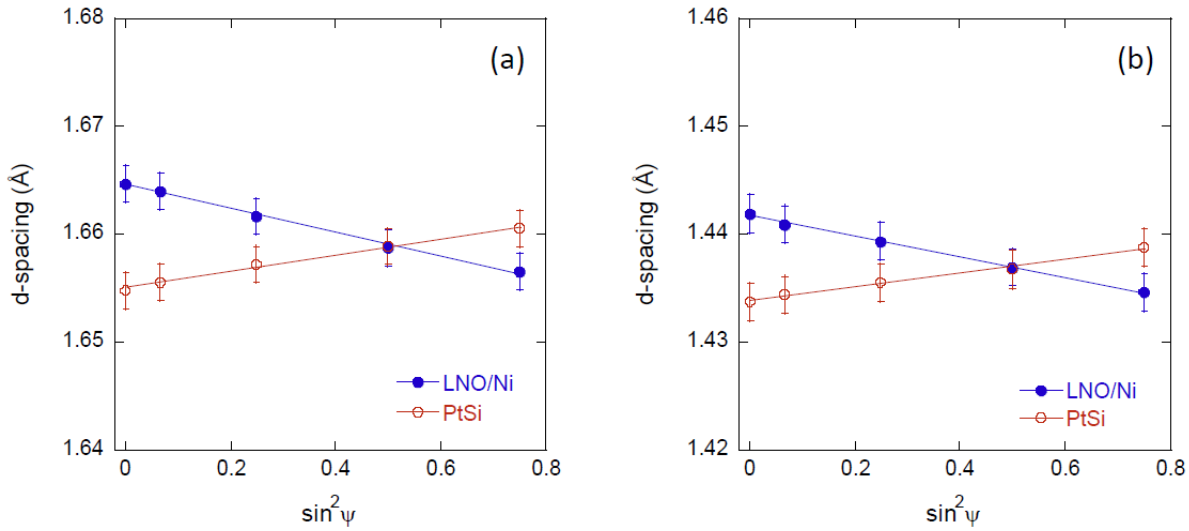

Figure 2. Lattice d-spacing as a function of $\sin^2\psi$ measured from (a) PLZT (211) and PLZT (220) diffraction peaks.

Figure 3a shows the dielectric constant and loss as a function of bias field measured at room temperature for samples of PLZT/LNO/Ni and PLZT/PtSi. The data conform to butterfly-shaped curves, which are typical for ferroelectric materials measured under the Curie temperature. At zero bias field, a dielectric constant of ≈1300 and dielectric loss of ≈0.06 were measured for PLZT/LNO/Ni, and a dielectric constant of ≈1350 and dielectric loss of ≈0.05 were found for PLZT/PtSi. Since both samples have PLZT films of the same thickness (≈2 μm) but grown on different substrates, they exhibit different field-dependent change, i.e., "tunability," which can be expressed as,

$$\tau = \left[1 - \frac{\varepsilon_r(E)}{\varepsilon_r(0)}\right] \times 100\% \qquad (2)$$

where ε_r(E) is the dielectric constant in the presence of an external field E.

We determined a tunability of ≈55% and ≈40% at room temperature under 100 kV/cm applied field for PLZT/LNO/Ni and PLZT/PtSi, respectively. This difference in tunability can be attributed to difference in residual stress for PLZT films grown on different substrates. Because the dipoles in PLZT film under compressive stress have better tendency of getting aligned in the out-of-plane direction, the dipole moment exhibits greater change collectively under a specific small change in applied field (or near zero field); but under high applied field, dipoles are more clamped and dipole moment is more difficult to change. For this reason, we measured sharper peaks in the butterfly curve of the dielectric constant as a function of applied field for PLZT/LNO/Ni and broader peaks for PLZT/PtSi.

Figure 3b shows the dielectric constant and loss measured at zero-bias field as a function of frequency for PLZT/LNO/Ni and PLZT/PtSi. The dielectric constant decreases while dielectric loss increases with increasing frequency for both samples. No obvious effect is observed due to different stress levels in the PLZT films grown on LNO/Ni and PtSi substrates.

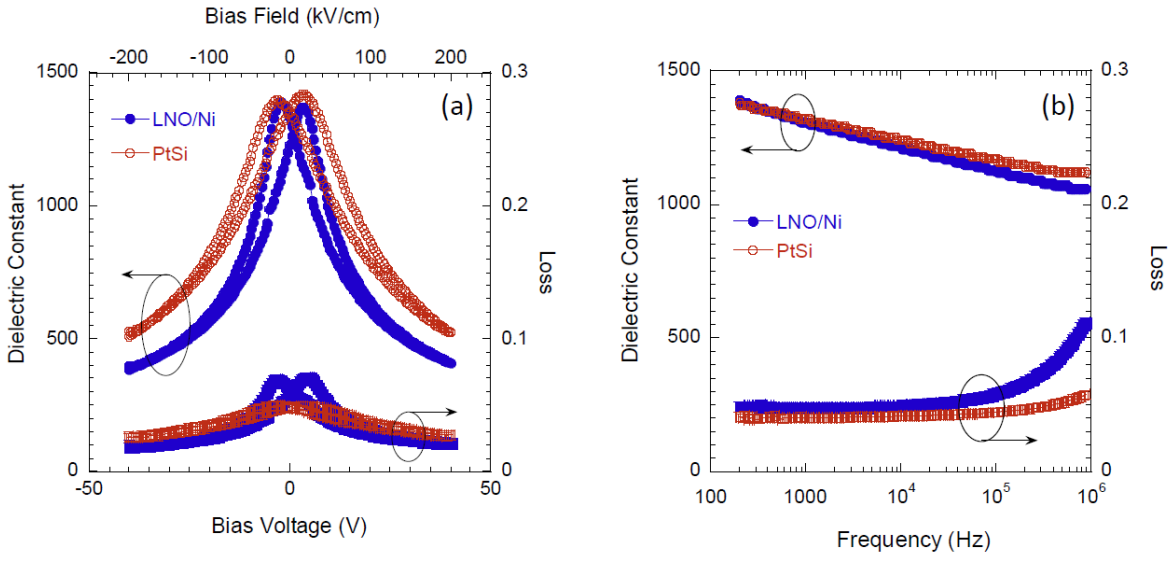

Figure 3. Dielectric properties of PLZT films (≈2-μm thick) grown on LNO/Ni and PtSi substrates as a function of (a) bias voltage and (b) frequency.

Figure 4 shows the polarization-electric field (P-E) hysteresis loops measured at room temperature on the PLZT/LNO/Ni and PLZT/PtSi. Both samples were coated with Pt top electrodes and measured with a field sweeping period of 10 ms (frequency of 100 Hz). Figure 5 shows the coercive field (E_c) and remanent polarization (P_r) as a function of maximum applied field (E_{max}) measured at room temperature on PLZT grown on LNO/Ni and PtSi substrates. Under the condition of maximum applied field >150 kV/cm, E_c of PLZT/LNO/Ni slowly increases with increasing maximum applied field (as shown in Fig. 5a), while that of PLZT/PtSi steadily increases with increase in applied field (Fig. 5b). Remanent polarization increases with increasing applied field for both PLZT/LNO/Ni and PLZT/PtSi. From the P-E loop with a maximum applied voltage of 50 V (corresponding to an electric field of 250 kV/cm), we measured a P_r of ≈23.5 μC/cm^2 and ≈7.4 μC/cm^2 and E_c of ≈25.6kV/cm and ≈21.1 kV/cm for PLZT/LNO/Ni and PLZT/PtSi, respectively. Even though the PLZT/LNO/Ni samples exhibit comparable coercive field when compared to the PLZT/PtSi samples, they display substantially higher remanent polarization. This difference in P-E loops can be attributed to the residual stress in PLZT films. Lee et al. [22] reported that both remanent polarization and saturation polarization decrease with an increase in tensile residual stress and increase with an increase in compressive stress (decrease in tensile stress), as in-plane compressive stress is beneficial to dipole alignment along the out-of-plane direction that is parallel to the applied field. Our experimental results revealed a similar trend.

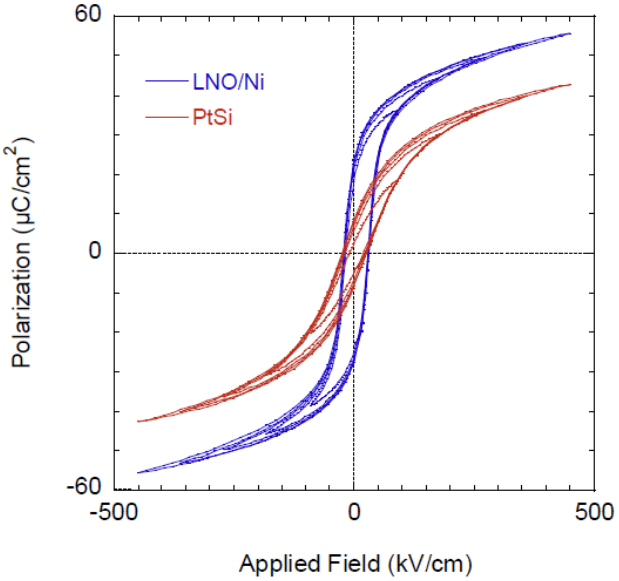

Figure 4. P-E hysteresis loops measured at room temperature on PLZT films (≈2-μm thick) grown on LNO/Ni and PtSi substrates.

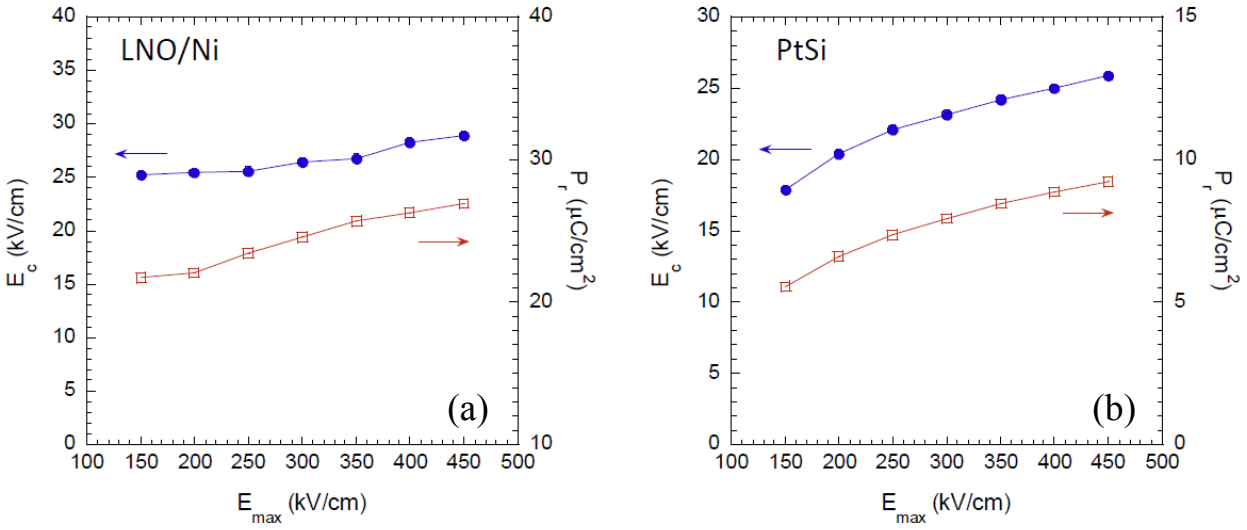

Figure 5. Coercive field and remanent polarization of PLZT (≈2-μm thick) grown on (a) LNO/Ni and (b) PtSi substrates measured at room temperature as a function of maximum applied field.

Sub-coercive field amplitude sweeps were performed as a function of frequency to investigate domain wall movements in the PLZT/LNO/Ni and PLZT/PtSi. The real part of permittivity (ε') increases with increasing AC field amplitude and decreases with increasing

frequency. It exhibits good linear dependence on the logarithm of frequency, as shown in Fig. 6, indicating that extrinsic factors such as motions of defect charge species and domain wall movement contribute to the polarization under low applied AC field. To quantitatively assess the contribution of the extrinsic effect on permittivity, we fitted ε' as a function of oscillation field amplitude E_0. As shown in Fig. 6 (inset), data measured at three frequencies (1 kHz, 10 kHz, and 100 kHz) fit well to the Rayleigh law [23],

$$\varepsilon' = \varepsilon'_{init} + \alpha' \cdot E_0 \qquad (3)$$

where ε', ε'_{init}, α', and E_0 are the real permittivity, initial (zero-field) permittivity, irreversible Rayleigh coefficient, and the applied AC oscillation field amplitude, respectively. It is worth noting that ε'_{init} consists of a combined reversible and intrinsic component to permittivity. The corresponding Rayleigh parameters derived from least square fitting of the experimental data to Eq. 3 are summarized in Table 1. The ratio of irreversible to reversible contributions to dielectric nonlinearity ($\alpha'/\varepsilon'_{init}$) that we measured for ≈2-μm-thick PLZT on PtSi substrates is in agreement with the reported literature values of 0.011 to 0.027 cm/kV for ≈2-μm-thick PZT films on PtSi substrates [24-26]. Bintachitt et al. investigated the nanoscale and mesoscopic disorder and associated local hysteretic responses in polycrystalline ferroelectric films and reported that large-scale collective domain wall dynamics, as opposed to motion of noninteracting walls, underpins the Rayleigh behavior in disordered ferroelectrics [26]. Bastani et al. reported the effect of PZT film thickness on dielectric nonlinearity [25]. They found the existence of a critical film thickness, ≈50 nm, below which the extrinsic contributions to the dielectric response are almost completely suppressed. Dielectric nonlinearity increases with film thickness because of increased interaction and collective movement of the domain walls [26]. The ratio of irreversible to reversible contributions we measured for PLZT/LNO/Ni is about twice as much higher than observed for PLZT/PtSi. This difference can be attributed to their difference in strain states; PLZT/ LNO/Ni bears ≈370 MPa compressive stress while PLZT/PtSi endures ≈250 MPa tensile stress. Compressive strain in PLZT films leads to enhanced polarization alignment and increased interaction among domain walls and, therefore, strengthened collective motion of domain walls under AC oscillation field.

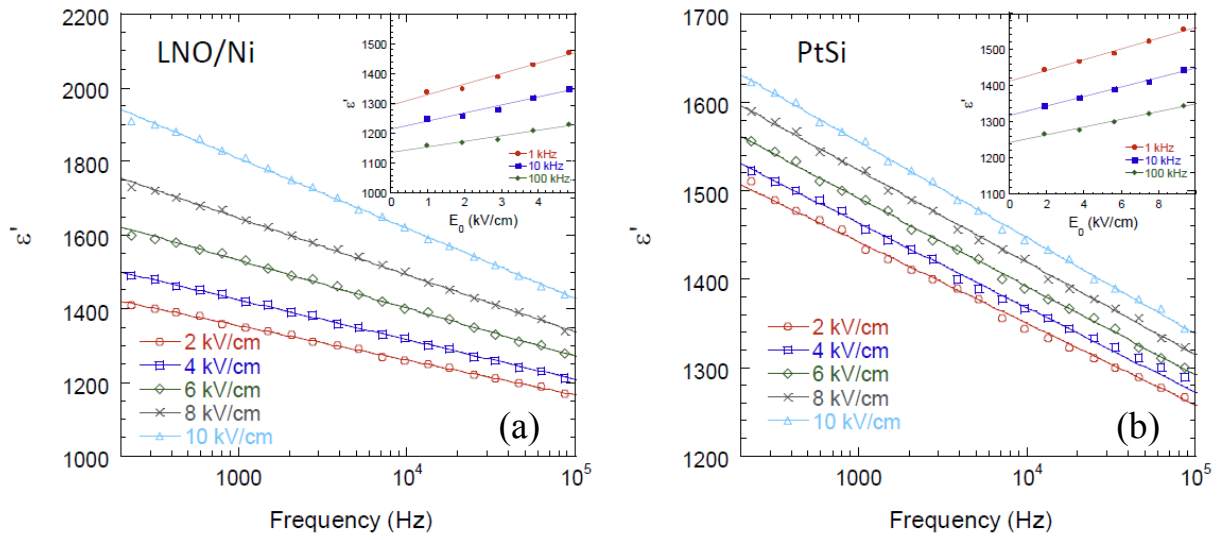

Figure 6. Frequency-dependent dielectric constant of PLZT films (≈2-μm thick) grown on (a) LNO/Ni and (b) PtSi substrates measured with various oscillation signal amplitudes; data plotted as function of oscillation signal amplitude are shown in corresponding insets.

Table 1. Rayleigh parameters of PLZT films (≈2-μm thick) grown on LNO/Ni and PtSi substrates.

Substrate	LNO/Ni			PtSi		
Frequency (kHz)	α' (cm/kV)	ε'_{init}	$\alpha'/\varepsilon'_{init}$ (cm/kV)	α' (cm/kV)	ε'_{init}	$\alpha'/\varepsilon'_{init}$ (cm/kV)
1	35.2	1294	0.027	14.8	1413	0.010
10	26.9	1214	0.022	13.1	1318	0.010
100	18.6	1136	0.016	10.7	1242	0.009

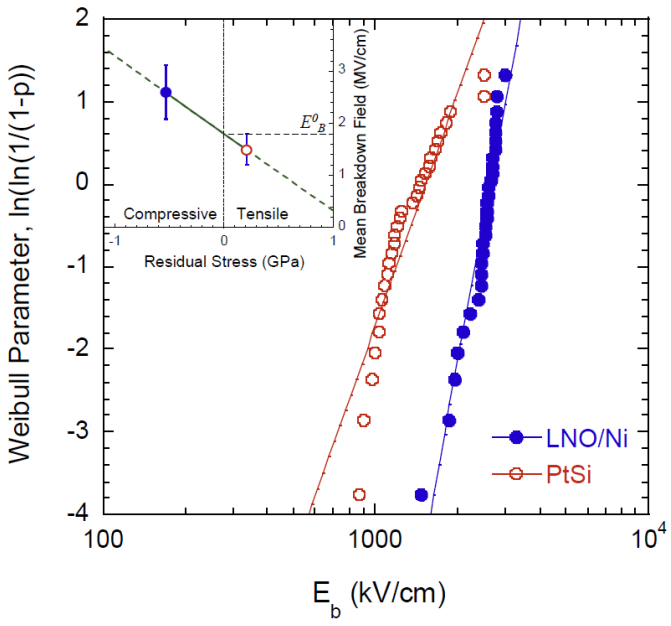

Figure 7. Weibull plot for breakdown field strength of PLZT (≈2-μm thick) deposited on LNO/Ni and PtSi substrates. Inset illustrates the correlation between mean breakdown field and residual stress.

Figure 7 shows the Weibull plot of breakdown field strength obtained at room temperature from 30 capacitor samples of PLZT/LNO/Ni and another 30 capacitor samples of PLZT/PtSi. The solid straight line is a least-square fitting to the two-parameter distribution function [27,28]. We measured mean breakdown field strengths of 2.6 MV/cm and 1.5 MV/cm for PLZT/LNO/Ni and PLZT/PtSi, respectively. The inset to Figure 7 illustrates the correlation between residual stress and PLZT film breakdown strength. Breakdown strength increases with decrease in tensile stress (or increase in compressive stress). When an electrical potential is applied between the top and the bottom electrodes, the electrostrictive strain causes expansion in the longitudinal direction (same direction as the applied electric field) and contraction in the radial direction (film in-plane direction). This condition leads to reduction in the overall compressive stress and/or addition in the overall tensile stress in PLZT films that are subjected to the applied field.

A "stress-free" breakdown strength (E_B^0) can be defined to facilitate the understanding of breakdown strength characteristics in PLZT films that are enduring residual stresses. When a preexisting tensile residual stress is present in a PLZT film, such as the one grown on a PtSi

substrate, the film needs less additional tensile strain to reach the threshold strain value that will cause dielectric breakdown. Therefore, this sample bearing residual tensile stress needs only an electric field of E_B^0 - ΔE_1 (with $\Delta E_1 > 0$) to reach the breakdown threshold value. For PLZT/ LNO/Ni, due to the existing compressive stress, additional field strength ΔE_2 is required to compensate the residual compressive strain. In other words, for the film to reach the threshold tensile strain level value that will cause dielectric breakdown, a total electric field of $E_B^0 + \Delta E_2$ (with $\Delta E_2 > 0$) must be applied. For this reason, we observed higher mean breakdown strength in PLZT films grown on LNO/Ni when compared to those grown on PtSi. This difference in breakdown strength is a direct result of the difference in residual stresses inside the PLZT/LNO/Ni and PLZT/PtSi. As illustrated in Fig. 7 (inset), E_B^0 can be determined from the intersection between the solid green line and the vertical line going through residual stress of zero. The E_B^0 value was found to be ≈1.8 MV/cm for the ≈2-μm-thick PLZT films grown by chemical solution deposition. The stress coefficient of the breakdown strength, determined from the slope of the solid line, was found to be -0.15 V·m/N. Therefore, it is beneficial to have a compressive residual stress in ferroelectric PLZT films for applications that require high field strength.

Figure 8a shows the P-E hysteresis loops of PLZT/LNO/Ni measured at room temperature with maximum applied voltages of 700 V, 800 V, and 900 V. The data reveal well-defined hysteresis curves with minimal enclosed areas. When electric field (E) applied to a ferroelectric film capacitor increases from zero to the maximum (E_m), the polarization (P) increases to the maximum (P_m), and the capacitor is thus charged with a total input energy density given by the following equation [6],

$$U_{Tot} = \int_0^{P_m} EdP \,. \qquad (4)$$

Upon discharging, the electric field decreases from E_m to zero; consequently, the stored energy is released with polarization decreasing from P_m to the remanent polarization P_r. The recoverable electric energy density is then expressed as,

$$U_{\mathrm{Rec}} = -\int_{P_m}^{P_r} EdP \,. \qquad (5)$$

With 900 V applied voltage (corresponding to an applied field of ≈4.5 × 10^6 V/cm), we measured a recoverable energy density of U_{Rec} ≈85 J/cm^3, as highlighted by the shaded area. This recoverable energy is by far the highest ever measured with PLZT film capacitors. The total input energy density (U_{Tot}), the recoverable energy density (U_{Rec}), and the energy conversion efficiency (η, defined as the ratio of recoverable energy density with respect to the total input energy density) are plotted in Fig. 8b as a function of maximum applied field E_{max}. Both U_{Rec} and U_{Tot} steadily increase and the conversion efficiency η slowly decreases with increasing E_{max}. We observed a recoverable energy density of U_{Rec} ≈85 J/cm^3 and conversion efficiency of ≈65% at room temperature with a maximum field of ≈4.5 MV/cm applied.

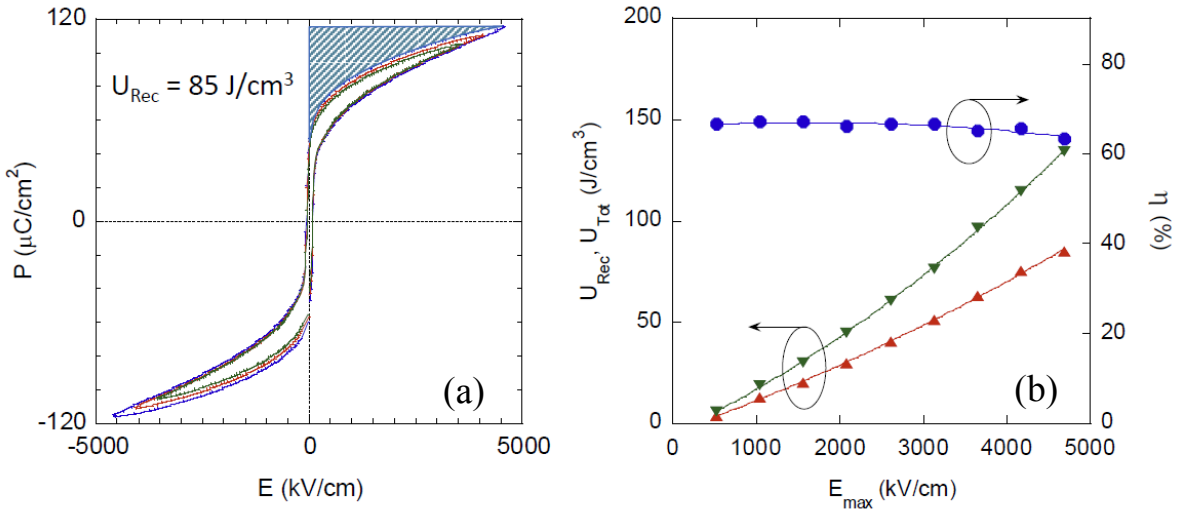

Figure 8. (a) High-field PE hysteresis loops and (b) U_{Rec}, U_{Tot}, and conversion efficiency η measured at room temperature with a PLZT film (≈2-μm thick) grown on LNO/Ni substrate.

Conclusions

In summary, we investigated the dielectric properties and energy storage performance of ≈2-μm-thick PLZT film capacitors grown on LNO/Ni and platinized silicon substrates. X-ray analysis revealed that the PLZT/LNO/Ni bears a compressive residual stress of ≈370 MPa while PLZT/PtSi endures a tensile residual stress of ≈250 MPa as a result of high-temperature crystallization heat treatment and mismatch in thermal expansion coefficients between the PLZT films and their substrates. The residual stress has profound effects on dielectric tunability,

ferroelectric hysteresis characteristics, domain wall movement, and dielectric breakdown strength. Compressive stress leads to heightened polarization, improved tunability, increased irreversible domain wall motion, and enhanced dielectric breakdown strength, all of which are desirable for high field applications. We observed a tunability of ≈55% and ≈40% at room temperature under 100 kV/cm applied field, P_r of ≈23.5 μC/cm^2 and ≈7.4 μC/cm^2, E_c of ≈25.6kV/cm and ≈21.1 kV/cm, and dielectric breakdown strength of ≈2.6 MV/cm and ≈1.5 MV/cm for PLZT/LNO/Ni and PLZT/PtSi, respectively. A U_{Rec} ≈85 J/cm^3 and η ≈65% were measured on PLZT/LNO/Ni at room temperature with a maximum applied field of ≈4.5 MV/cm. Our results reveal the potential of using PLZT film capacitors for power electronics and energy storage applications.

Acknowledgment

This work was funded by the U.S. Department of Energy, Vehicle Technologies Program, under Contract No. DE-AC02-06CH11357. Microstructure analysis was accomplished at the Electron Microscopy Center for Materials Research at Argonne National Laboratory, a U.S. Department of Energy Office of Science Laboratory operated under Contract No. DE-AC02-06CH11357 by UChicago Argonne, LLC.

References

[1] C.-B. Eom, S. Trolier-McKinstry, "Thin-film piezoelectric MEMS," *MRS Bulletin* **37** (2012)1007-1017.

[2] S. Kwon, W. Hackenberger, E. Alberta, E. Furman, M. Lanagan, "Nonlinear dielectric ceramics and their applications to capacitors and tunable dielectrics," *IEEE Electrical Insulation Mag.* **27** (2011) 43.

[3] P. Kim, N. M. Doss, J. P. Tillotson, P. J. Hotchkiss, M.-J. Pan, S. R. Marder, J. Li, J. P. Calame, J. W. Perry, "High energy density nanocomposites based on surface-modified $BaTiO_3$ and a ferroelectric polymer," *ACS Nano* **3 (**2009) 2581-2592.

[4] X. Hao, J. Zhai, L. B. Kong and Z. Xu, "A comprehensive review on the progress of lead zirconate-based antiferroelectric materials," *Progress in Materials Science* **63** (2014) 1-57.

[5] B. Chu, X. Zhou, K. Ren, B. Neese, M. Lin, Q. Wang, F. Bauer, Q. M. Zhang, "A dielectric polymer with high electric energy density and fast discharge speed," *Science* **313** (2006) 334-336.

[6] Z. Hu, B. Ma, R. E. Koritala, U. Balachandran, "Temperature-dependent energy storage properties of antiferroelectric $Pb_{0.96}La_{0.04}Zr_{0.98}Ti_{0.02}O_3$ thin films," *Appl. Phys. Lett.* **104** (2014) 263902.

[7] S. A. Rogers, "FY13 Annual Progress Report for the Advanced Power Electronics and Electric Motors Program," US DOE/EE-1040, Washington, DC (2013).

[8] B. Rangarajan, B. Jones, T. Shrout, M. Lanaga, "Barium/lead-rich high permittivity glass-ceramics for capacitor applications," *J. Amer. Ceram. Soc.* **90** (2007) 784-788.

[9] K. Yao, S. Chen, M. Rahimabady, M. S. Mirshekarloo, S. Yu, F. E. H. Tay, T. Sritharan, L. Lu, "Nonlinear dielectric thin films for high-power electric storage with energy density comparable with electrochemical supercapacitors," *IEEE Trans. on Ultrasonics, Ferroelectrics, and Frequency Control* **58** (2011) 1968-1974.

[10] B. Ma, D. K. Kwon, M. Narayanan, U. Balachandran, "Dielectric properties and energy storage capability of antiferroelectric $Pb_{0.92}La_{0.08}Zr_{0.95}Ti_{0.05}O_3$ film-on-foil capacitors," *J. Mater. Res.* **44** (2009) 2993-2996.

[11] X. Hao, Y. Wang, J. Yang, S. An, J. Xu, "High energy-storage performance in $Pb_{0.91}La_{0.09}(Ti_{0.65}Zr_{0.35})O_3$ relaxor ferroelectric thin films," *J. Appl. Phys.* **112** (2012) 114111.

[12] B. Ma, M. Narayanan and U. Balachandran, "Dielectric strength and reliability of ferroelectric PLZT films deposited on nickel substrates," *Mater. Lett.* **63** (2009) 1353-1356.

[13] K. D. Budd, S. K. Dey, D. A. Payne, "Sol–gel processing of $PbTiO_3$, $PbZrO_3$, PZT, and PLZT thin films," *Proc. Br. Ceram. Soc.* **36** (1985) 107-121.

[14] B. Ma, D. K. Kwon, M. Narayanan,U. Balachandran, "Chemical solution deposition of ferroelectric lead lanthanum zirconate titanate films on base-metal foils," *J. Electroceram.* **22** (2009) 383-389.

[15] B. Ma, D. K. Kwon, M. Narayanan,U. Balachandran, "Leakage current characteristics and dielectric breakdown of antiferroelectric $Pb_{0.92}La_{0.08}Zr_{0.95}Ti_{0.05}O_3$ film capacitors grown on metal foils," *J. Phys. D: Appl. Phys.* **41** (2008) 205003.

[16] C. K. Kwok, S. B. Desu, "Pyrochlore to perovskite phase transformation in sol-gel derived lead-zirconate-titanate thin films," *Appl. Phys. Lett.* **60** (1992) 1430-1432.

[17] Q. Zou, H. E. Ruda and B. G. Yacobi, "Improved dielectric properties of lead zirconate titanate thin films deposited on metal foils with $LaNiO_3$ buffer layers," *Appl. Phys. Lett.* **78** (2001) 1282-1284.

[18] B. Ma, S. Liu, S. Tong, M. Narayanan, U. Balachandran, "Enhanced dielectric properties of $Pb_{0.92}La_{0.08}Zr_{0.52}Ti_{0.48}O_3$ films with compressive stress," *J. Appl. Phys.* **112** (2012) 114117.

[19] P. S. Prevéy, "X-ray Diffraction Residual Stress Techniques," in *Metals Handbook*, Metals Park, OH, American Society for Metals (1986) 380-392.

[20] R. J. Ong, D. A. Payne, N. R. Sottos, "Processing effects for integrated PZT: Residual stress, thickness, and dielectric properties," *J. Am. Ceram. Soc.* **88** (2005) 2839-2847.

[21] G. A. C. M. Spierings, G. J. M. Dormans, W. G. J. Moors, M. J. E. Ulenaers, P. K. Larsen, "Stress in Pt/Pb(Zr,Ti)O_3/Pt thin-film stacks for integrated ferroelectric capacitors," *J. Appl. Phys.* **78** (1995) 1926-1933.

[22] J. Lee, C. Park, M. Kim H. Kim, "Effect of residual stress on the electrical properties of PZT films," *J. Am. Ceram. Soc.* **90** (2007) 1077-1080.

[23] D. Damjanovic and M. Demartin, "The Rayleigh law in piezoelectric ceramics," *J. Phys. D: Appl. Phys.* **29** (1996) 2057-2060.

[24] N. Bassiri-Gharb, I. Fujii, E. Hong, S. Trolier-McKinstry, D. V. Taylor, D. Damjanovic, "Domain wall contributions to the properties of piezoelectric thin films," *J. Electroceram.* **19** (2007) 49-67.

[25] Y. Bastani, T. Schmitz-Kempen, A. Roelofs, N. Bassiri-Gharb, "Critical thickness for extrinsic contributions to the dielectric and piezoelectric response in lead zirconate titanate ultrathin fil," *J. Appl. Phys.* **109** (2011) 014115.

[26] P. Bintachitt, S. Jesse, D. Damjanovic, Y. Han, I. M. Reaney, S. Trolier-McKinstry, S. V. Kalinin, "Collective dynamics underpins Rayleigh behavior in disordered polycrystalline ferroelectrics," *Proc. Natl. Acad. Sci. U.S.A.* **107** (2010) 7219-7224.

[27] W. Weibull, "A statistical distribution function of wide applicability," *J. Appl. Mech.* **18** (1951) 293-

297.
[28] L. A. Dissado, "Theoretical basis for the statistics of dielectric breakdown," *J. Phys. D: Appl. Phys.* **23** (1990) 1582-1591.